Journal of Nuclear Materials 547 (2021) 152728

Contents lists available at ScienceDirect

Journal of Nuclear Materials

journal homepage: www.elsevier.com/locate/jnucmat

Modelling fission gas behaviour in fast reactor $(U,Pu)O_2$ fuel with BISON

Filippo Verdolin[a], Stephen Novascone[b,*], Davide Pizzocri[a], Giovanni Pastore[b,c], Tommaso Barani[a], Lelio Luzzi[a]

[a] Politecnico di Milano, Department of Energy, Nuclear Engineering Division, via La Masa 34, I-20156 Milano, Italy
[b] Computational Mechanics and Materials Department, Idaho National Laboratory, Idaho Falls, ID 83415, USA
[c] Department of Nuclear Engineering, University of Tennessee, Knoxville, TN 37916, USA

ARTICLE INFO

Article history:
Received 10 July 2020
Revised 27 November 2020
Accepted 7 December 2020
Available online 8 January 2021

Keywords:
Nuclear fuel
MOX
Fast reactors
Finite element method
Fission gas behaviour

ABSTRACT

The physics-based fission gas behaviour model available in the BISON fuel performance code provides satisfactory predictive capabilities for application to light-water reactor conditions. In this work, we present a model extension for application to fast reactor $(U,Pu)O_2$ fuel. In particular, we detail the introduction of a lower bound to the number density of grain-face bubbles, representing a limit to the coalescence process once extensive bubble interconnection is achieved. This new feature is tested first against an experimental database for UO_2-LWR, and secondly is validated against integral irradiation experiments for fast reactor $(U,Pu)O_2$ fuel rods irradiated in the FFTF (Fast Flux Test Facility) and in the JOYO reactors. The comparisons of BISON results with the experimental data are satisfactory and demonstrate an improvement compared to the standard version of the code.

© 2020 Elsevier B.V. All rights reserved.

1. Introduction

Uranium-plutonium mixed oxide fuels (MOX) are candidate fuels for several fast reactor concepts [1,2]. Fast reactor conditions pose $(U,Pu)O_2$ fuels under considerable load in terms of high-temperature, steep-temperature gradients and extended burnup [1,3]. In view of this difference in the operation conditions, the behaviour of fission gas in fast reactor $(U,Pu)O_2$ fuels is different from that of UO_2 in light-water reactors (LWR)[4–6].

A sufficiently high-temperature gradient can induce the formation of a central void in the fuel pellet [3,7]. The central void forms due to the migration up the temperature gradient of porosity left over from sintering [3,7,8]. Also, the migration of the pores leads to fuel restructuring, exhibiting the formation of new regions within the fuel. In particular, besides the central void, we can identify three other main regions within fast reactor $(U,Pu)O_2$ fuels (Fig. 1), characterized by different microstructures [7]:

- In the inner region of the fuel column where the temperature is high enough, the fuel undergoes restructuring driven by an evaporation/condensation mass transport across fabrication pores [1,3,9,10]. In the restructured area, columnar grains are formed, exhibiting lower grain-boundary retention of fission gas than in the unrestructured region because of the cylindrical shape of the columnar grains.
- In the intermediate region, after the restructuring, the microstructure of the fuel is characterized by equiaxed grains [1,3].
- The outer region is unaltered. In this outer region, the pores do not move because of the low temperature.

Due to this difference in microstructure and in consideration of the high-temperature level in the fast reactor $(U,Pu)O_2$ fuel, attempting to directly apply fission gas behaviour models tailored to UO_2 in LWRs is usually not straightforward [12]. For example, difficulty arises from the fact that higher temperature implies (exponentially) faster kinetics of diffusive processes governing fission gas behaviour, resulting in a range of model solutions for fission gas release (FGR) and swelling typically not achieved in LWR conditions. It is worth noticing that conservative approaches assuming high temperatures and traditionally applied as design criteria are not acceptable predictive models to be applied in fuel performance simulations (e.g., used for the conservative design of the plenum free volume). It has been shown with best-estimate calculation (e.g., see Ref. [13].) that operational fission gas release in prototype lead-cooled and lead-bismuth-eutectic-cooled fast reactors is in the range of 20 to 60%, i.e., much higher than typical values for LWRs but well below the 80–90% observed in sodium-cooled fast reactors for power production [1]. Also, the range of 80–90%

* Corresponding author.
E-mail address: stephen.novascone@inl.gov (S. Novascone).

https://doi.org/10.1016/j.jnucmat.2020.152728
0022-3115/© 2020 Elsevier B.V. All rights reserved.

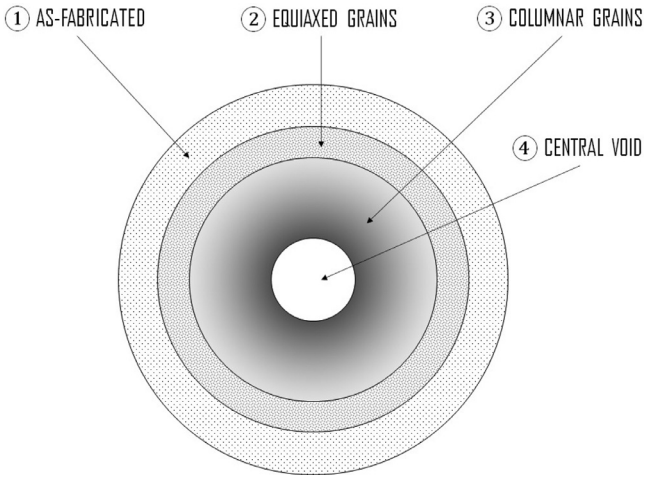


Fig. 1. Diagram of microscale features where the region after restructuring are distinguished. For more detailed images and information, see Ref. [11].

of release refers to past generations of sodium-cooled fast reactors, because of their higher temperature target, while, for the new generation sodium-cooled fast reactors, it is lower. On the other hand, Lead Fast Reactors (LFRs) and Lead Bismuth eutectic fast reactors (LBE-FRs) operates at lower temperatures; therefore, their FGR is also lower. For these reasons, the development of predictive models for fission gas behaviour in fast reactor $(U,Pu)O_2$ fuel is a key point for the effective application of fuel performance codes, hence, it is targeted by several research programs, like [14–16].

In this work, we present a version of the model by Pastore et al. [17,18], which was originally developed and validated for LWR UO_2, adapted to the description of fission gas behaviour in fast reactor $(U,Pu)O_2$. In particular, we propose the introduction of a physics-based limit to the process of coalescence of growing grain-boundary bubbles. We implemented the modified version of the model into the BISON fuel performance code [19] and we verified, for local[1] analyses, the behaviour of this extension to the model against the experimental database presented by Baker [20,21]. Subsequently, we validated the extended version of the model against integral irradiation experiment performed in fast reactors. It is worth noting that there are other phenomena linked to the FGR that do not depend strictly on the diffusion and the evolution of the gas bubbles, but they are connected to the fuel stoichiometry, the Plutonium content and species mobility. Also, the gas diffusion coefficient used in this work, i.e. Turnbull [22], may not be reliable because it has been developed for UO_2 at LWR conditions. For these reasons, we know that all these phenomena are particular to $(U,Pu)O_2$ irradiated in fast reactors and the model of Pastore [18], tailored on UO_2 at LWR conditions, does not account for these phenomena. Therefore, the scope of this work is to show that a model for fission gas behaviour developed for LWR conditions with few improvements could have a good reproducibility of the results for $(U,Pu)O_2$ irradiated in fast reactors. However, this work represents an initial extension and other important phenomena that affect FGR (like stoichiometry, Plutonium content, species migration) will be considered in future work.

The outline of this paper is as follows. In Section 2, we briefly summarize the main model equations and we detail the proposed modifications. In Section 3, the modified model is tested for local analyses of UO_2 fuel irradiation at temperatures covering both LWR and FBR (Fast Breeder Reactor) ranges. In Section 4, the modified model is tested for the simulation of integral irradiation experiments under fast reactor conditions with BISON, and results are compared to experimental data.

[1] With local analysis and simulation, we mean a simulation using a simplified fuel-only model with a single-cube mesh, in order to simulate the local behaviour of the model in small fuel samples.

2. Model description

In this section, we briefly summarize the main model equations and we detail the proposed modifications. In the second part, we discuss some fundamental assumptions and parameters that affect the simulated fission gas behaviour.

2.1. Model development

According to the model of Pastore et al. [17,18] fission gas behaviour is described as comprised of two main components, i.e., the intra-granular and inter-granular stages. The intra-granular part of the model can be summarized as follows.

Fission gas atoms generated in the fuel grains diffuse towards the grain boundaries through the processes of trapping into and re-solution from nanometer-size intra-granular gas bubbles. The gas arriving at the grain-faces precipitates into grain-face gas bubbles, responsible for grain-face swelling. Fission gas diffusion from within the fuel grain (assumed as spherical) to the grain boundary in one-dimensional spherical geometry is described by:

$$\frac{\partial C}{\partial t} = D_{\text{eff}} \frac{1}{r^2} \frac{\partial}{\partial r} \left(r^2 \frac{\partial C}{\partial r} \right) + \beta \tag{1}$$

where C (atoms m^{-3}) is the intra-granular gas concentration (as single atoms in dynamic solution with the matrix and in bubbles), t (s) is the time, r (m) is the radial coordinate in the spherical geometry, β (atoms m^{-3} s^{-1}) is the gas generation rate, D_{eff} (m^2 s^{-1}) is the effective gas diffusion coefficient from Speight [23].

The inter-granular part of the model involves the concurrent calculation of gaseous fuel swelling due to grain-face bubbles and fission gas release, through a description of grain-face bubble development [17,18]. In summary, an initial number density of grain-face bubbles, N_0 (bubbles m^{-2}), is considered with further nucleation during irradiation being neglected (one-off nucleation). Bubbles are assumed to have lenticular shape of circular projection on the grain faces and to all have the same size at any instant. The absorption rate of gas atoms at bubbles is considered to equal the arrival rate at grain boundaries from Eq. 1. The phenomenon of growth (or shrinkage) of grain-face bubbles is described by Pastore et al. [17] referring to the model of Speight and Beere [24]. The overpressurization of the gas bubbles is the driving force of the vacancy absorption/emission mechanism:

$$\frac{\mathrm{d}n_v}{\mathrm{d}t} = k(p - p_{\text{eq}}) \tag{2}$$

where n_v (vacancies bubble^{-1}) is the number of vacancies per bubble, k is a kinetic constant depending (exponentially) on temperature and on the geometry of the grain face (see White [25]), p and p_{eq} (Pa) are the pressure of the gas in the bubble and the mechanical equilibrium pressure, respectively. The gas pressure is calculated based on the number of gas atoms and vacancies in each bubble and using the van der Waals equation of state [17]. Bubble growth leads the grain-face bubbles to interconnect and merge into larger but fewer bubbles. This coalescence process is described, using a modified model of White [25], relating the rate of decrease of the bubble number density, N (bubble m^{-2}), due to coalescence to the rate of increase of bubble projected area on the grain-face, A (m^2)

$$\frac{\mathrm{d}N}{\mathrm{d}t} = \frac{6N^2}{3 + 4NA} \left(\frac{\mathrm{d}A}{\mathrm{d}t} \right) \tag{3}$$

Hence, the coalescence process results in progressively fewer, larger bubbles. When the bubbles reach a sufficient level of interconnection, the grain face is considered as percolated and the fission gas is released to the fuel rod free volume through free pathways made of interconnected bubbles. In the model of Pastore et al. [17], this is underpinned by a principle of grain-face saturation: after the fractional coverage $F = NA$ has reached the saturation value F_{sat}, further bubble growth is compensated by gas release in order to maintain the constant coverage condition:

$$\frac{dn_{FGR}}{dt} = 0 \quad \text{if} \quad F < F_{sat}$$
$$\frac{dn_{FGR}}{dt} = n\frac{N}{A}\frac{dA}{dt} \quad \text{if} \quad F = F_{sat} \tag{4}$$

where n_{FGR} (atoms m^{-2}) is the number of gas atoms released to the fuel rod free volume per unit grain-boundary surface and n (atoms bubble^{-1}) the number of fission gas atoms per grain-face bubble. The saturation point is assumed as a constant with a value of $F_{sat} = 0.5$ [17,18,25].

The model by Pastore et al. [17] is currently the default option in BISON [19], and has been extensively validated in LWR UO_2 cases [27,17,18,26]. It is expected that for (U,Pu)O_2 fuels irradiated in fast reactors this model requires modifications and further validation.

In fact, it has been demonstrated [5,28] that fission gas release reaches high values (outside of the current validation range of the model) at high temperatures often achieved by (U,Pu)O_2 fuels irradiated in fast reactors. In these conditions, the kinetic constant k in Eq. 2 becomes large, resulting in bubbles rapidly growing by diffusion-driven absorption of gas atoms and vacancies. As a consequence of bubble growth, the bubble number density strongly decreases, governed by Eq. 3.

Nevertheless, there should be a physical limit to the coalescence process, i.e., bubble growth would not result in noticeable further reduction of the number of bubbles once extensive interlinkage is attained. In a simple approach, this limit can be interpreted as a lower bound to the number density of grain-face bubbles. In the original BISON model, such a lower bound was set to a constant value of 10^{10} bubbles m^{-2} [18]. However, this limit is of low importance for LWR fuel calculations, where it is normally not attained. On the contrary, for the analysis of higher temperature fuel such as (U,Pu)O_2 fuels irradiated in fast reactors in which bubble growth and coalescence proceed more rapidly, the limit becomes highly important in determining the calculated FGR and gaseous swelling.

In this work, we further develop the concept of a lower bound for the number density of grain-face bubbles and propose a physically grounded approach to its determination.

Assuming a spherical grain of radius a (m), it has a surface area of $4\pi a^2$ (m^2). Idealizing the surface area as divided into a number of grain faces n_{face}, each face has an area of

$$A_{face} = \frac{4\pi a^2}{n_{face}}. \tag{5}$$

Considering that each grain face is shared by two grains, and considering a number of equivalent bubbles per grain face n_{eq}, we can express the bubble number density as

$$N = \frac{1}{2}\frac{n_{eq}}{A_{face}} = \frac{1}{2}\frac{n_{eq}n_{face}}{4\pi a^2}. \tag{6}$$

With this notation, the limit number density of grain-face bubbles per unit surface, N_{lim} (bubbles m^{-2}) is

$$N_{lim} = \frac{1}{2}\frac{n_{eq,lim}n_{face}}{4\pi a^2} \tag{7}$$

where $n_{eq,lim}$ (bubbles face^{-1}) is the average number of bubbles on a grain face when the saturation of bubbles is reached. The estimation of this parameter is obtained via a random numerical experiment detailed in the following subsection. As for the number of faces per grain n_{face}, it is assumed to be 14, based on the number of faces of a tetradecahedron.

2.2. Random numerical experiment for the derivation of the bubble equivalent number

In this section, we describe the process used for the derivation of the bubble equivalent number, $n_{eq,lim}$. In order to determine a range of reasonable values for the bubble equivalent number, we performed a numerical experiment. The goal of this experiment is just the derivation of the bubble equivalent number and not the bubble evolution itself because we are aware of the limitations of this derivation in describing such a complex phenomenon.

This numerical experiment presents the following characteristics:

- We generate 1000 square images representative of the grain-faces.
- Each grain face is assumed of size 10x10 μm^2.
- On each grain face, we generate overlapping single-sized circles of radius R sampled from an uniform distribution $R(\mu\text{m}) \sim \mathcal{U}[0, 1]$.
- In each grain face, we count the effective number of bubbles, i.e., the number of not-connected clusters of circles.

For this numerical experiment, we considered that the exact size of the grain face is not relevant for the determination of the proposed lower bound to bubble number density since it is expressed in terms of density[2]. Nevertheless, the assumed size of the grain face corresponds to a grains radius of 10 μm. This can be determined by approximating the 3D shape of the grain with a sphere of surface $4\pi a^2$. If one assumes it is divided into 14 faces of 100 μm^2 each, a corresponds to a value of 10 μm.

Also, both bubbles centres coordinates are sampled from uniform distributions. Bubbles ending up close to the edge are simply trimmed by the edge. We are not interested in catching edge-effects, such as percolation of the grain face, and hence the shape of the edge does not represent a strong limitation to our conclusion.

In principle, given enough trials, the patterns generated with bubbles of different size will be covered also by single-size bubbles (with a higher number of smaller single-size bubbles, i.e., the increase in trials required).

We are aware that overlapping circles is a partial representation of bubble coalescence, missing the relaxation of edges which could be represented by phase-field models [29,30]. On average, both the phase field and the overlapping circles are a reasonable representation of the experimental data[3].

In Fig. 2a, the effective number of bubbles is reported as a function of the fractional coverage F, with each point representing one of the 1000 images generated. The number of effective pores gradually decreases with the increase of the fractional coverage, because of coalescence. As an example, Fig. 2b reports one of the images generated, with fractional coverage $F = 0.43$ and a number of effective bubbles $n_{eq} = 29$. From Fig. 2a, in conditions of saturation, i.e., when $F = F_{sat} = 0.5$, n_{eq} is in the range 0–20 bubbles face^{-1}. In this work, we assume[4] $n_{eq,lim} = 10$. Moreover, comparing

[2] This assumption holds if the square is big enough compared to the bubble size.

[3] This comparison is performed on the vented fraction, and we are careful in claiming its generality, but we believe it is an indication of the viability of our "geometrical" approach.

[4] It should be clarified that the bubble concentration we are considering in our model is independent on the grain size, whereas the absolute number of bubbles is consequently proportional to the grain surface area. This assumption is justified by

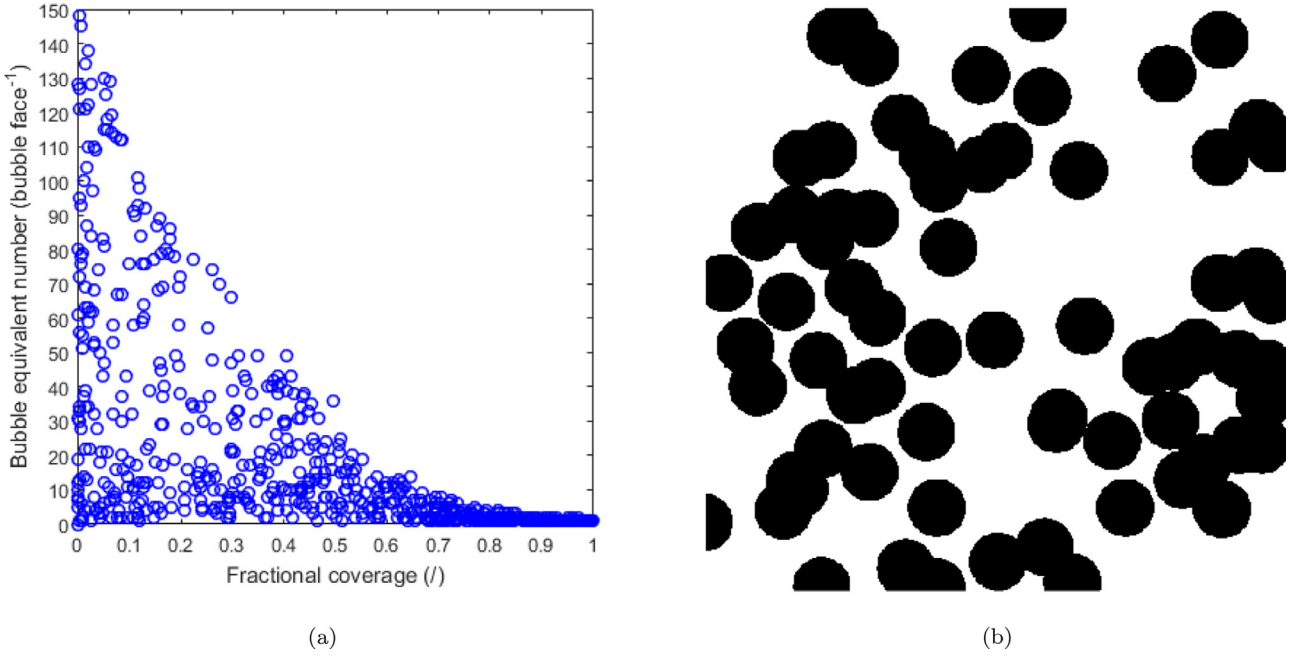


Fig. 2. Results of the random numerical experiment used to derive the number of equivalent bubbles per grain face. On the left (a) we report the bubble equivalent number obtained as a function of the fractional coverage, while on the right (b) we report a sample image of a pattern of bubbles covering a grain face as obtained by the random process.

N_{lim} with the range observed bubble densities at saturation, one can note that the proposed limit in this work is compatible with experimental observations of saturated grain boundaries[5], see Ref. [25].

The inclusion in the BISON fission gas behaviour model of a lower bound to the inter-granular bubble density bounds the coalescence process and, once the lower limit for the number density of bubbles is achieved, any further bubble growth is compensated by FGR by virtue of Eq. 4, and both bubble number density and size remain constant. Note that in the current model, given the same fractional coverage, the fewer the bubbles the larger the volume they occupy and the higher the total gas atoms they retain [17,18]. Hence, FGR after the attainment of the limit is expected to be higher compared to the situation where coalescence continues.

After the attainment of the lower limit in the number density of grain-face bubbles, in the model, the grain-face bubble population is assumed to reach a stationary situation where further evolution is prevented. Also, after extensive interlinkage, bubbles form elongated or vermicular structures [25], so that the basic model assumption of circular bubbles becomes stronger in itself. However, the concept of a stationary situation is considered reasonable as an attempt to consider behaviour after extensive bubble interlinkage within the current model framework and in a physically meaningful way. As a final physical justification for the introduction in the model of such a lower bound, it should be observed that without any limitation the evolution of grain-face bubbles ignores the fact that bubbles are constrained on a single grain face, and can in principle allow for interconnection between bubbles belonging to different grain faces.

2.3. Modeling assumptions and parameters

An important parameter that affects FGR is the single gas atom diffusion coefficient. The default intra-granular single gas atom diffusion coefficient used in BISON standard version was provided by Turnbull et al. [31] neglecting the contribution of the athermal term (D_3). However, for the simulations with the extended model, we decided to use the single gas atom diffusion coefficient proposed by Turnbull et al. [22]. We decided to use the original complete diffusion coefficient proposed by Turnbull [22] as it is since it is the reference coefficient used in most similar models in the state of the art. This diffusion coefficient is described as follows:

$$D_s = D_1 + D_2 + D_3 \tag{8}$$

where D_1 (m^2 s^{-1}) is the thermal component that depends just on temperature, D_2 (m^2 s^{-1}) the irradiation-enhanced term that is a function of both temperature and the fission rate and D_3 (m^2 s^{-1}) is the athermal component depending only on the fission rate. It has been decided to use the coefficient proposed by Turnbull et al. [22] because this diffusion coefficient emphasizes the enhanced and the athermal components dependent on the fission rate.

In addition, another issue related to the simulation of fast reactor (U,Pu)O_2 cases with BISON pertains to the grain growth. BISON only incorporates an UO_2-LWR model [32], which is not suitable to represent grain growth under FBR conditions. Hence, for this work, because of the lack of a model able to describe the grain growth for these conditions, it has been decided to use constant values for the grain radius[6]. We are aware that the restructuring of oxide

the fact that we do not consider grain growth and therefore the grain size of the problem is fixed as an initial condition. This modelling choice arises from the fact that classical grain growth models are barely applicable in the temperature range of the fuels considered in this work. This implies that the resulting "grain size" referred to in our work is more a modelling abstract quantity than a physical variable representative of the real grain size.

[5] The values for N_{lim} used in sections 3 and 5 fall in the range of 0.9–270 $\times$ 10^{11} bubbles m^{-2} observed by White [25]. It is important to keep in mind that the values of N_{lim} (from 5.6 $\times$ 10^{10} bubbles m^{-2} to 3.5 $\times$ 10^{11} bubbles m^{-2} for a grain radius of 10 and 4 μm, respectively) are related to saturation conditions, i.e. at a fractional coverage of 0.5 because this model feature becomes relevant when the saturation of grain boundaries has been reached. However, the data by White [25] are taken from fuel irradiated and ramped in conditions which may not be representative of a fast reactor environment, therefore we are inclined to consider this comparison as indicative and not a strong support of the proposed new parameter.

[6] We assumed the grain radius as constant in time and uniform along the pellet radius. This abstract modelling assumption is to be intended just for the modelling

fuel in fast reactor conditions determine a dramatic change in the crystalline structure [3,9], as mentioned in the introduction of this work. Indeed, the inclusion of a consistent model for grain growth, fuel restructuring and their influence of fission gas behaviour will be the subject of future investigations.

An investigation about the effects of the grain radius on the limit described in Eq. 7 is performed in Section 5.

3. Model test with local simulations with BISON

In this section, we assess the impact of the lower bound of bubble number density introduced via Eq. 7 on the fission gas behaviour model of Pastore et al. [17,18] at different temperatures. The assessment is carried on analyzing the experimental database from Baker (Ref. [20,21]). In these experiments, the fuel pins have been irradiated in the UKAEA's Winfrith SGHWR up to a burnup of ∼1% and the samples examined by Baker (Ref. [21], [20]) lay in the temperature range from 1273 K up to 2073 K. Therefore, these values represent both operational conditions for UO_2-LWR (up to about 1600 K) and more critical ones (beyond 1700 K), closer to operational conditions of (U,Pu)O_2 fuel irradiated in fast reactors.

The experimental data from [20,21] correspond to local information, i.e., small fuel samples from irradiated rods. In order to simulate local behaviour with BISON, we used a single-cube mesh. Every simulation has been performed at a different temperature (starting from 1273 K up to 2073 K, consistent with the Baker database) and assuming a typical value[7] for the grain radius, i.e., 5 μm, corresponding to a N_{lim} of 2×10^{11} bubbles m^{-2}, coming from Eq. 7.

Figs. 3 and 4 report all the results at each of the considered temperatures for the quantities of most interest, namely: the fission gas release *FGR* (%), the number density of grain boundary bubbles per unit surface *N* (bubbles m^{-2}) and the volumetric swelling due to grain-boundary bubbles (%). The results are shown for both standard and modified BISON. At lower temperatures (Fig. 3), since the bubble number density at the grain boundaries *N* does not reach the proposed limit N_{lim}, the resulting *FGR* and volumetric swelling at the grain boundary are the same in both the cases. In Fig. 4, as temperature raises (from 1773 K and so on), the lower bound for the bubble number density at the grain boundary proposed in this work is attained (Figs. 3a, 3d, 3g and 3j) and this implies a higher *FGR* and a lower volumetric swelling at the grain boundary compared to the standard BISON case.

The swelling prediction we observe at high temperature is higher than that observed by White [25]. This is to be expected, since the irradiation histories which end up with swellings around 7% are the result of 5ı500 hours of irradiation at 1800°C, while the irradiations considered by White are characterized by slightly higher temperatures but only for ramps of short duration. The irradiation time at high temperature is the principal reason behind the difference in the two values of swelling. In fact, due to the higher temperatures (comparable to ranges for fast reactor (U,Pu)O_2 fuel), the associated pronounced bubble growth and coalescence lead to the attainment of the lower bound for the number density of grain boundary bubbles systematically.

These results highlight the impact of the proposed model modification at temperatures comparable to fast reactor fuel conditions.

4. Integral fuel rod analyses

The integral irradiations simulated[8] in the present work are taken from the experiments FO-2 [33,34], MK-I and MK-II [35]. The FO-2 assembly has been irradiated in the Fast Flux Test Facility (FFTF), a sodium fast reactor, for 312 equivalent full power days (EFPD) [33] between December 22, 1984, and April 25, 1986, to a peak burn-up of ∼6% FIMA (Fissions per Initial Metal Atom) and a peak fast fluence of 9.9×10^{22} n cm^{-2} (E > 0.1 MeV) [34]. This test uses the alloy HT-9 as cladding material. The FO-2 assembly is composed by 169 fuel pins of twelve different types. The fuel was manufactured with co-precipitated (U,Pu)O_2 powder, ensuring a uniform plutonium distribution throughout the pellets [34]. The annular fuel[9] pin L09 was destructively examined. This pin was punctured and it was cut at three different elevations.

JOYO was the first sodium-cooled reactor leading the FBR development program in Japan. MK-I core has been irradiated in the Japanese experimental fast reactor JOYO at 50 MW_t and at 75 MW_t from 1977 to 1981 [35], up to a burnup of ∼2.5% FIMA and ∼5% FIMA, respectively. MK-II core was irradiated in the JOYO reactor from 1983 to 1986, up to a burnup of ∼5% FIMA. The MK-I and MK-II cores are composed by a maximum of 80 and 67 driver assemblies, respectively, surrounded by stainless steel reflectors.

More details about the power histories and other information for the experiments FO-2 and MK can be found in Teague et al. [34] and Shimada et al. [35], respectively. The specifications for these experiments are summarized in Table 1[10].

5. Calculation results

In this section, we show the results of integral rod simulations and a sensitivity analysis about the impact of the grain size on the results.

5.1. Integral rod simulation results

In this Section, we present the calculation results of integral rod simulations obtained with BISON. In Figs. 5(a)-5(d) two different cases have been examined:

- A first case that considers the standard version of BISON;
- A second case that takes into account the lower limit for the bubble number density at the grain boundary N_{lim} (Eq. 7) dependent on the grain radius proposed in this work with the single gas atom diffusion coefficient presented by Turnbull et al. [22].

As shown in Figs. 5(a)-5(d), one can observe that introducing N_{lim} according to Eq. 7 the fission gas release prediction is closer to the experimental data. These results indicate that the limitation introduced describes better the physical limit of grain-face bubble interconnection occurring at typical operational conditions for fast reactor (U,Pu)O_2 fuel. However, in some cases, the results are not in a good agreement with the experimental data (e.g Fig. 5(b) at a burnup lower than 1% FIMA). In this case, the onset is not well described by the model. The reason could be because further modelling developments are required to take into account other phenomena (like stoichiometry and Plutonium content and distribution) that affect the FGR.

of fission gas behaviour and should not be intended as a general model representative of the fuel microstructure.

[7] This consideration might be correct for equiaxed grains, but here we are not considering the cylindrical grains.

[8] Phenomena like oxygen defects are outside of the scope of this work, although their impact on the overall behaviour of fast reactor fuel and on fission gas behaviour is relevant.

[9] Furthermore, the effect of open porosity, due to an annular pellet or to the formation of a central void, is not taken into account because the fission gas behaviour model implemented in BISON operates by point.

[10] The provided power refers to a simplified power history from Teague et al. [34] and it is representative of the average value.

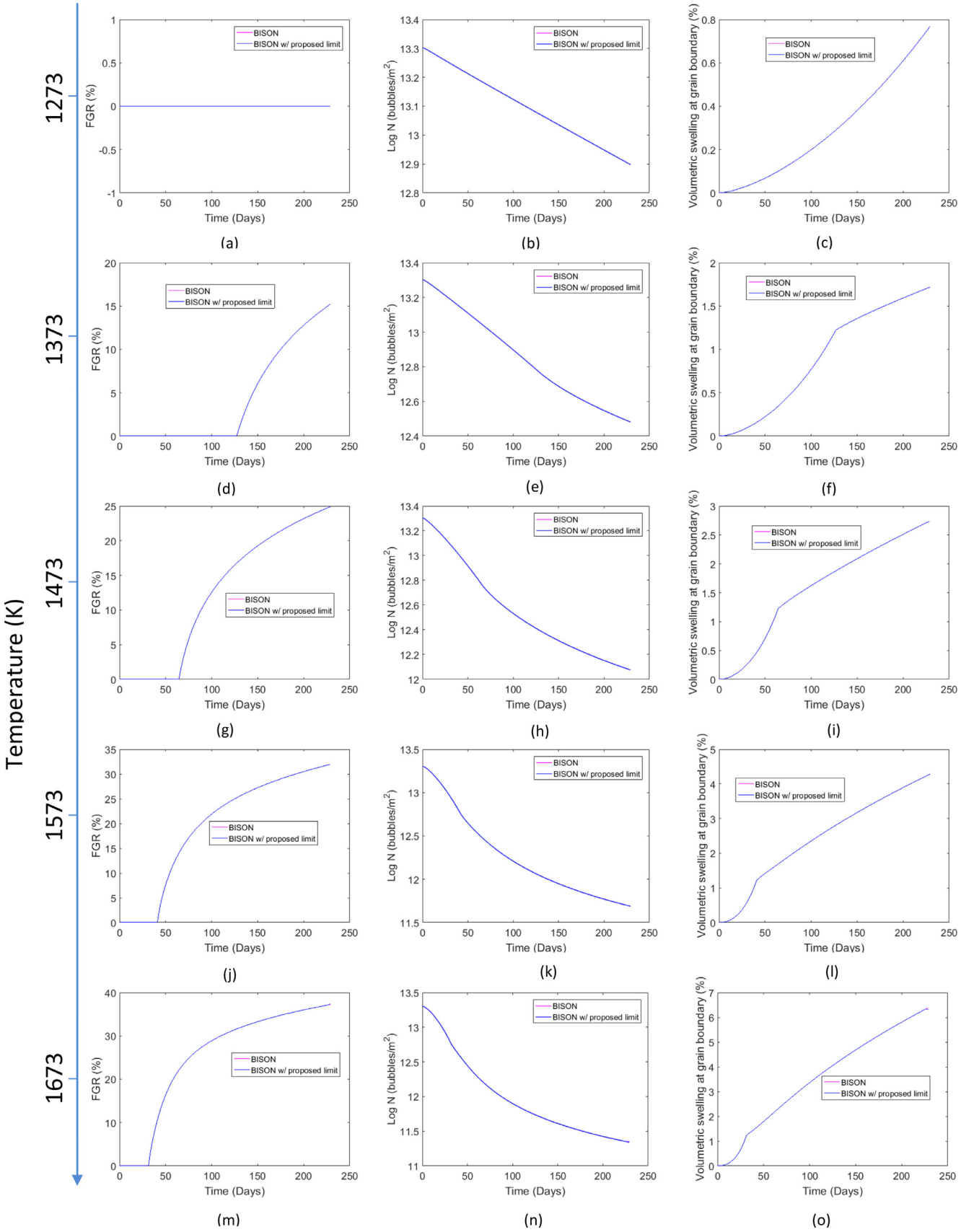


Fig. 3. Local simulations on UO_2 from the Baker database ([21] and [20]) performed with BISON in a range of temperatures from 1273 K up to 1673 K. For every temperature the fission gas release *FGR* (%), the number density of bubbles at the grain boundary per unit surface N (bubbles m^{-2}) and the volumetric swelling at the grain boundary (%) evolution as a function of the time are reported. The plots related to N are expressed with a semi-logarithmic scale. In every figure, the purple lines, corresponding to the standard BISON version, cannot be distinguished from the blue ones (with a N_{lim} of 2×10^{11} bubbles m^{-2}, coming from Eq. 7), because they are overlapped. (For interpretation of the references to colour in this figure legend, the reader is referred to the web version of this article.)

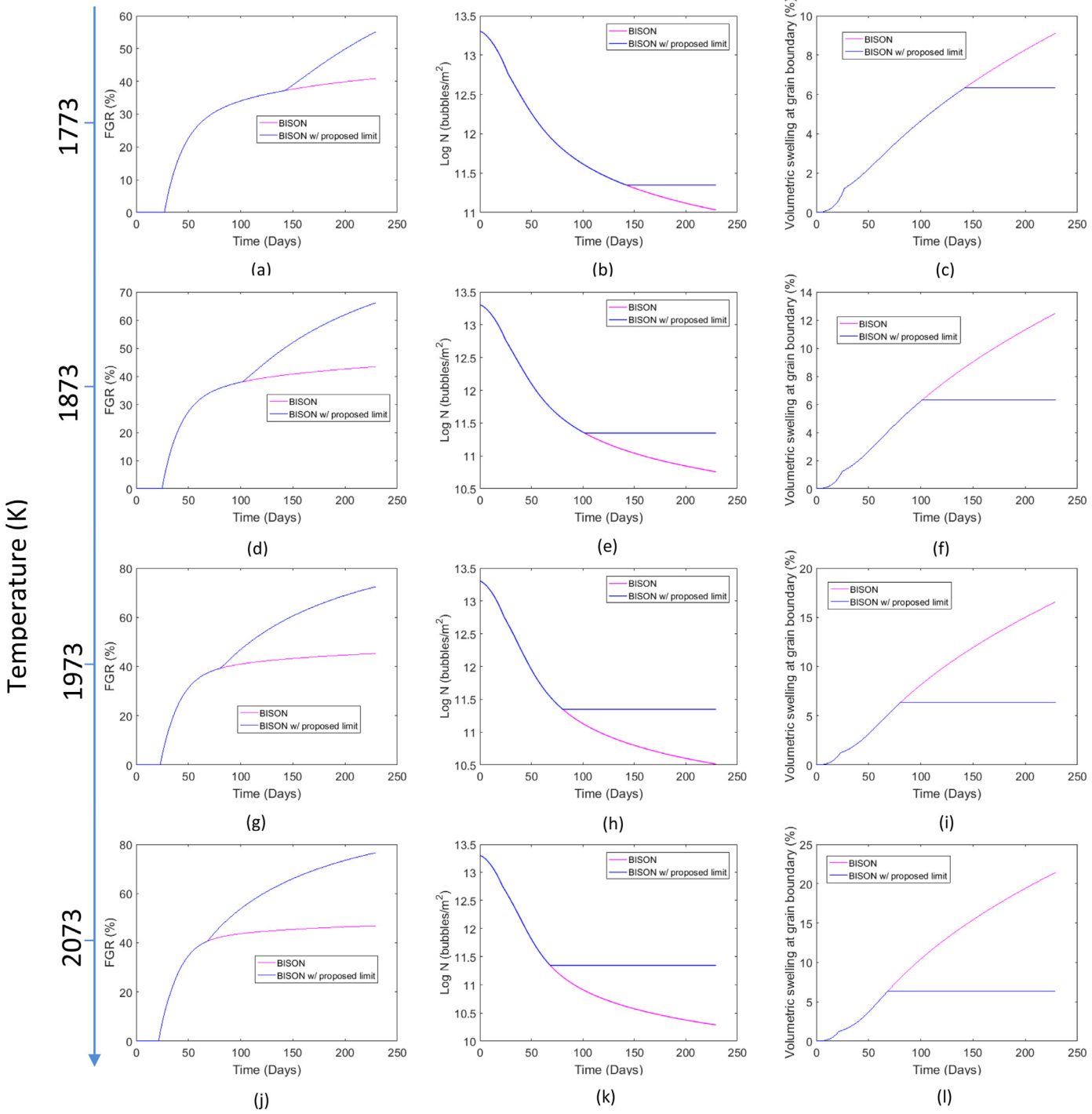


Fig. 4. Local simulations on UO_2 from the database [21] and [20] performed with BISON in a range of temperatures from 1773 K up to 2073 K. For every temperature the fission gas release *FGR* (%), the number density of bubbles at the grain boundary per unit surface *N* (bubbles m^{-2}) and the volumetric swelling at the grain boundary (%) evolution as a function of the time are reported. The plots related to *N* are expressed with a semi-logarithmic scale in order to highlight the differences between the two cases analyzed. The purple line refers to the standard BISON version; the blue line refers to the case that uses the lower bound for the bubble number density at the grain boundary N_{lim} (Eq. 7), corresponding to a value of 2×10^{11} bubbles m^{-2}. (For interpretation of the references to colour in this figure legend, the reader is referred to the web version of this article.)

Also, the quality of the results could be affected by the use of some parameters that have been developed for LWR conditions, first of all, the gas diffusion coefficient. The relationship provided by Turnbull [22] may not be accurate enough to describe this phenomenon under such different conditions (e.g. higher temperatures, different microstructure, different stoichiometry).

In order to discuss the effect of grain-size on the results, we propose a sensitivity analysis with an analytical approach. This analysis was performed concerning the model illustrated by Pastore et al. [17,18].

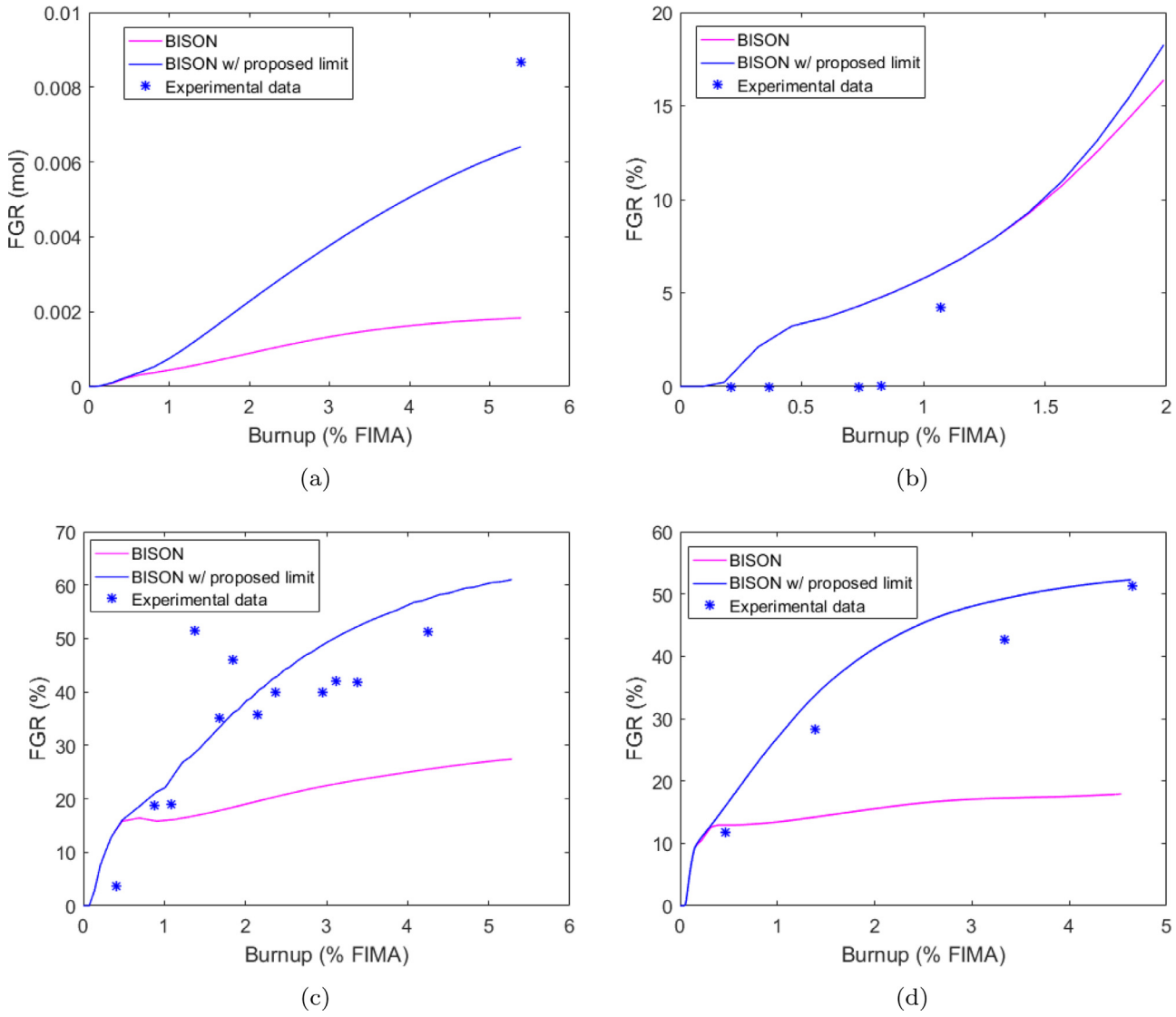


Fig. 5. Calculation results for *FGR* compared with experimental irradiation data. The purple line refers to the standard BISON version; the blue line corresponds to the case that uses the lower limit for the bubble number density at the grain boundary N_{lim} (Eq. 7). Fig. 5a refers to the fuel pin L09 from the FO-2 assembly, assuming a constant grain radius of 10 μm, value reported by [34]. The consequent N_{lim} corresponds to a value of 5.6×10^{10} bubbles m^{-2}. Figs. 5b-5 c show the results for MK-I core irradiated at 50 MW_t and at 75 MW_t respectively, while the simulations for MK-II core are illustrated in Fig. 5d. Figs. 5b-5 d, related to JOYO reactor, refer to a constant grain radius of 8 μm [36], with N_{lim} corresponding to a value of 8.7×10^{10} bubbles m^{-2}. (For interpretation of the references to colour in this figure legend, the reader is referred to the web version of this article.)

Table 1
Fuel pin specifications and irradiation data.

Rod	FO-2 L09	MK-I at 50MW_t	MK-I at 75MW_t	MK-II
Fuel Data				
Fuel material	$(U,Pu)O_2$	$(U,Pu)O_2$	$(U,Pu)O_2$	$(U,Pu)O_2$
PuO_2 content (wt%)	26.0	18	18	30
Pellet outer diameter (mm)	5.59	5.4	5.4	4.63
Pellet inner diameter (mm)	1.397	-	-	-
Fuel stack height (mm)	914	600	600	550
Pellet density (%TD)	91.7	93.5	93.5	93
Fuel Rod				
Cladding material	HT-9	316SS	316SS	316SS
Cladding outer diameter (mm)	6.858	6.3	6.3	5.5
Cladding thickness (mm)	0.533	0.35	0.35	0.35
Gap width (μm)	101.6	100	100	100
Nominal plenum height (mm)	1057	600	600	550
Fill gas composition	He	He	He	He
Fill gas pressure (MPa)	0.1	0.3	0.3	0.3
Linear heat rate (kW m^{-1})	38.8[8]	21	32	40
Max. Burnup (% FIMA)	~6	~2.5	~5	~5

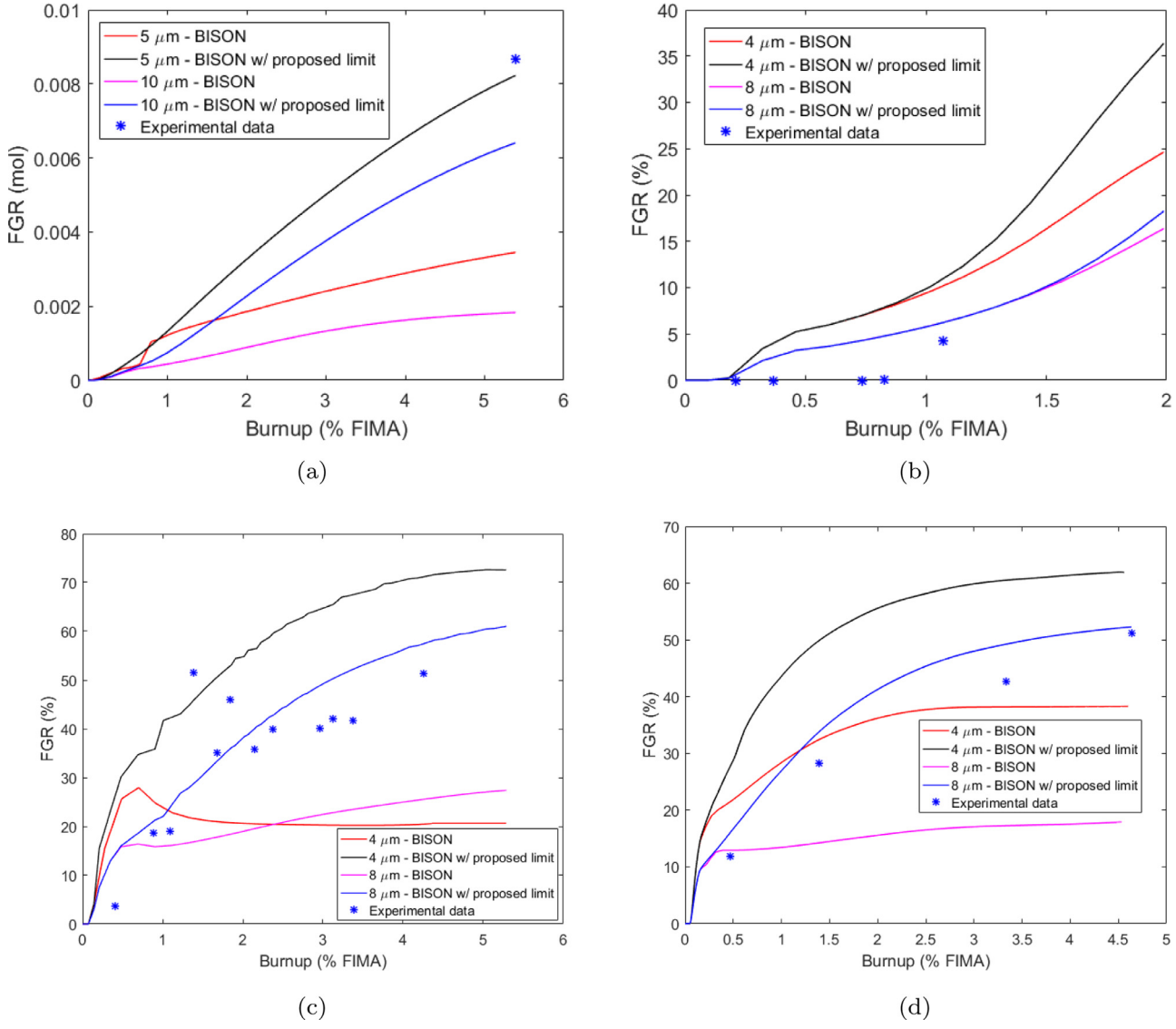


Fig. 6. Sensitivity analysis performed varying the grain radius in a realistic range after the restructuring (from 4 to 10 μm). Fig. 6a refers to the fuel pin L09 from the FO-2 assembly (grain radius of 5 and 10 μm, with N_{lim} corresponding to 2×10^{11} and 5.5×10^{10} bubbles m^{-2}, respectively); Figs. 6b-6 c show the sensitivity analysis for MK-I core irradiated at 50 MW$_t$ and at 75 MW$_t$ respectively, while the simulations for MK-II core are illustrated in Fig. 6d (grain radius of 5 and 10 μm, with N_{lim} corresponding to 3.5×10^{11} and 8.7×10^{10} bubbles m^{-2}, respectively).

5.2. Sensitivity analysis

In this section, we want to add more value to our work, performing a sensitivity analysis study. However, the sensitivity analysis is not the main goal of this work, and this study will be investigated more deeply in future publications. To see the effects on the final release due to the perturbation, generated adding a quantity δC of gas[11], it is necessary to linearize[12] the equations (presented by Pastore et al. [17,18] and seen in Section 2) that govern the fission gas behaviour. Hence, once linearized, Eq. 1 that describes the intra-granular diffusion becomes:

$$\frac{\partial \delta C}{\partial t} = D_{\text{eff}} \frac{1}{a} \frac{\partial^2 \delta C}{\partial r^2}\bigg|_a \tag{9}$$

Eq. 9 shows an inverse proportionality between the diffusion phenomenon and the grain radius a. In fact, the larger the grain, the longer the average diffusion path to the grain boundary.

After linearizing all the equations governing the grain boundary gas behaviour Eqs. 2–(4) presented by Pastore et al. [17], referring to the fractional coverage $F = F_{\text{sat}} = 0.5$ (/) as stationary steady-state point and adding a δC as perturbation to the system, one obtains:

$$\delta n_{\text{FGR}}\Big|_{N_{\text{lim}}} = \frac{n_{\text{sp}} N_{\text{sp}}}{A_{\text{sp}}} \left[\left(\omega + \frac{2\pi D_v \delta_g}{\Omega S n_{v_{\text{sp}}}} t \right) \left(\frac{\delta C}{3 N_{\text{sp}}} a \right) \right]^{2/3} \tag{10}$$

where δn_{FGR} (atoms m^{-2}) is the variation of number of fission gas atoms released to the fuel rod free volume after the perturbation, assuming a constant value of N_{lim}, n_{sp} (atoms bubble^{-1}) is the number of fission gas atoms per grain-face bubble in the stationary point, N_{sp} (bubbles m^{-2}) is number density of grain-face bubbles

[11] The scope of the model is limited to fission gas behaviour and does not consider several fundamental effects yet, which are therefore not included in the sensitivity.

[12] The overall model is highly non-linear, and linearization is to be done carefully. In our analysis, the linearization is to be intended in the proximity of a set of the state variables of the model and used only for perturbation purpose. In the proximity of the set of state of variables values, the linearization is thus a legitimate approximation.

per unit surface in the stationary point, A_{sp} (m^2) is the projected area of grain-face bubbles, ω (m^3) is the van der Waals volume of a fission gas atom, D_v (m^2 s^{-1}) is the vacancy diffusion coefficient on grain boundaries, δ_g (m) is the thickness of the diffusion layer in grain boundaries, Ω (m^3) is the atomic (vacancy) volume in grain-boundary bubbles, S (-) is a model parameter (that depends on the fractional coverage) calculated in Pastore et al. [25], $n_{v_{sp}}$ (vacancies bubble^{-1}) is the number of vacancies per grain-face bubble in the stationary point, and t (s) is the time.

Performing a derivative of Eq. 10 with respect to the grain radius a, one can obtain:

$$\left.\frac{\partial \delta n_{FGR}}{\partial a}\right|_{N_{lim}} = \frac{n_{sp}N_{sp}}{A_{sp}}\left[\left(\omega + \frac{2\pi D_v \delta_g}{\Omega S n_{v_{sp}}} t\right)\left(\frac{\delta C}{3N_{sp}}\right)\right]^{2/3}\left(\frac{2}{3a^{1/3}}\right) \tag{11}$$

in which it is neglected that the proposed N_{lim} depends on the grain size itself Eq. (7). Eq. 10 points out a dependence of the *FGR* to the rod free volume of $a^{2/3}$. This effect is due to the decrease of the surface-to-volume ratio of the grain with the increase of the grain radius a. Looking at the derivative (Eq. 11) one can observe that this process is limited since the $\partial \delta n_{FGR}/\partial a$ follows a law proportional to $a^{-1/3}$. Hence, with larger grains, the surface-to-volume ratio decreases and this increases grain boundary storing capacity. When many gas atoms are stored in the grain boundaries, the release does not depend on the intra-granular diffusion anymore (Eq. 9) but just on the law described in Eq. 10. This can happen just when many gas atoms are stored in the grain boundaries, and only after a certain burnup level. As the release threshold is reached, there is an expected impact of the proposed N_{lim} value on the concentration of gas being released. This impact is quantitatively evaluated by considering the variation of N_{lim} with the grain size a, namely:

$$\frac{\partial N_{lim}}{\partial a} = -\frac{n_{eq.lim} n_{face}}{4\pi a^3}. \tag{12}$$

After the lower bound to the inter-granular bubble number density is reached, the coalescence process described by Eq. 3 is considered to stop. This calls for a different expression of the linearized equations governing the grain boundary gas behaviour, resulting in

$$\delta n_{FGR} = \frac{n_{sp}}{A_{sp}}\left[\left(\omega + \frac{2\pi D_v \delta_g}{\Omega S n_{v_{sp}}} t\right)\left(\frac{\delta C}{3N_{sp}} a\right)\right]^{2/3} N_{lim} \tag{13}$$

$$\frac{\partial \delta n_{FGR}}{\partial a} = \frac{n_{sp}}{A_{sp}}\left[\left(\omega + \frac{2\pi D_v \delta_g}{\Omega S n_{v_{sp}}} t\right)\left(\frac{\delta C}{3N_{sp}}\right)\right]^{2/3}\left(\frac{2}{3}a^{2/3}\right)\frac{\partial N_{lim}}{\partial a}. \tag{14}$$

Thus after the lower bound $N = N_{lim}$ is reached, there is an impact of the proposed model parameter on the overall fission gas release. By comparing Eqs. 11 and 14, we can observe that

- The amount of gas released from the grain boundaries is proportional to the proposed lower bound for the bubble density (considering a linear approximation of model equations). Higher values used for this parameter, e.g., considering higher number of bubbles per grain face or higher number of faces per grain, hence imply a higher predicted fission gas release.
- The dependency on the grain size of the proposed lower bound, expressed by Eq. 12, implies that the expected dependency of the fission gas release on the grain radius changes after the lower bound is reached.

Since the grain radius a is the only free parameter involved in the definition of the lower bound N_{lim}, we reported in Table 2 the dependency of the discussed figures of merit on the grain radius itself, clarifying the change in dependency between the predicted fission gas release with/without considering any lower bound (i.e., after/before the lower bound is eventually reached). It is worth noting that after the lower bound is reached, the predicted fission gas release becomes monotonically decreasing with the grain radius since higher grain radius correspond to lower values of the proposed lower bound (Eq. 7).

After this analytical study, we also investigated the effect of the grain-size on the results performing additional simulations. Fig. 6 shows a comparison between the case using the current version of BISON and the one with N_{lim} proposed in this work, also considering two different constant values of grain radius: 5 and 10 μm for the L09 pin; 4 and 8 μm for MK-I and MK-II cores. These values lie in the range that goes from 4 to 10 μm referred to a realistic size for the grain characteristic dimension after the restructuring (Ainscough et al. [32]). Looking at Fig. 6, one can make some observations.

- The *FGR* for the cases using the limitation N_{lim} with a lower grain radius (black line) is higher than in the case with a higher grain radius (blue line). A smaller grain leads to a shorter average diffusion path to the grain boundary.
  Hence, due to this intra-granular diffusion effect (Eq. 1), in a smaller grain, more gas atoms will reach the grain boundary and will be released. This effect can be easily observed also in Table 2. In this table, we report the dependency on the grain radius for both the behaviours (intra-granular and inter-granular).
- In Figs. 6(a)-6(b) the intra-granular diffusion effect (Eq. 9) prevails again (red line versus purple line) on the surface-to-volume effect described for the grain boundary gas behaviour (Eq. 10), see also Table 2. Hence, in a smaller grain, more gas can reach the grain boundary and then can be released. However, Fig. 6c shows that this is valid only until a certain value of burnup (the purple line crosses the red one). After a certain burnup level, the grain boundary storing capability becomes dominant: many gas atoms are already stored in the grain boundary and ready to be released. As shown by Eq. 10, this storing capability is improved with larger grains.
- Again up to a certain burnup (approximately ~1.5% FIMA) the case with N_{lim} with a larger grain (blue line) has a lower release compared to the case with no limitations and with a smaller grain (red line). This shows that up to that burnup the intra-granular effect is stronger, but beyond the grain boundary storing capacity becomes the dominant effect. Furthermore, one can notice that the approaching of the bubble number density lower limit, where (from Eq. 7) it corresponds to a value of 2×10^{11} bubbles m^{-2}, improves the release for the case represented by the blue line. Consequently, once the lower limit for the number density of bubbles is achieved, any further bubble growth is compensated by FGR. This is shown in Fig. 6(a) and Fig. 6(c), while in Fig. 6(b) a sufficiently high level of burnup is not reached.

6. Conclusion and future work

The main goal of this work was modelling fission gas behaviour in fast reactor (U,Pu)O_2 fuel with BISON. A model for the calculations of fission gas behaviour was already included in BISON. However, this model was validated only for LWR cases so far. We proposed a new physics-based limit to represent conditions of extended bubble growth and interlinkage at grain boundaries that occur at high temperatures (typical conditions achieved during irradiation in FBRs). Therefore, the scope of this work is to show that a model for fission gas behaviour developed for LWR conditions with few improvements could have a good reproducibility of the results for (U,Pu)O_2 irradiated in fast reactors. However, we are

Table 2
Summary of the sensitivity analysis about the dependency on the grain radius for intra-granular and inter-granular behaviour.

Scenarios	Figure of merit	Dependency on grain radius, a
Intra-granular behaviour	Variation of intra-granular gas concentration, δC	$\delta C \sim a^{-1}$
Inter-granular behaviour w/o proposed limit	Variation of fission gas released, δn_{FGR}	$\delta n_{\mathrm{FGR}} \sim a^{2/3}$
Inter-granular behaviour w/ proposed limit	Variation of fission gas released, δn_{FGR}	$\delta n_{\mathrm{FGR}} \sim a^{-4/3}$

aware that many other phenomena that affect FGR (like stoichiometry, Plutonium content, species migration) are relevant and they should be considered in future work. We applied the extended model to local simulations (i.e., performed using a simplified fuel-only model with a single-cube mesh) in order to prove the importance of the limit. Hence, we applied the model to integral FBR $(U,Pu)O_2$ fuel rod simulations with BISON demonstrating a marked improvement in the FGR predictions compared to the standard version of BISON. In particular, the results point out that at low temperatures the grain-face bubble growth and the consequent coalescence are far from their physical limits, while at higher ranges those limiting effects occur. Also, the sensitivity analysis performed highlights the strong dependency of the FGR on the grain size. In conclusion, according to the results obtained in this work, the extension to the fission gas behaviour model provides an improved representation of fission gas behaviour under fast reactor conditions. Future efforts can be invested in the validation of the proposed model against more irradiation cases, and in the analysis of other kinds of $(U,Pu)O_2$ fuels as well. For example, the model could be improved taking into account the heterogeneity effect of the MOX fuels, due to the presence of plutonium agglomerates, on the fission gas release. This feature becomes very important in the modelling of MOX fuel irradiated in thermal reactors. This could be done implementing into the present model the outcomes from the studies of Koo et al. [12] and of Ishida and Korei [37].

A further perspective for future work regards the effect of open porosity to the release. The model describes the release by point, but it could be improved to consider also inner surfaces due to the formation of a central void or because the fuel pin is annular.

Another open issue is the development of a grain growth model able to describe better this phenomenon at high temperatures, especially after the restructuring in order to define also the columnar grain region. So far, all the grains have been considered as spheres, but this approximation can be valid only for as-fabricated and equiaxed grain regions. The columnar grains, instead, present a cylindrical shape, hence, in this case, all the equations involved should be described with cylindrical coordinates. This improvement could be also useful for the sensitivity analysis prospect because a grain growth model can feed directly the expression presented in this work for the N_{lim}, which can be adopted for a more accurate sensitivity analysis. However, the sensitivity analysis is not the main goal of this work, and this study will be investigated more deeply in future work, taking into account other parameters and phenomena besides the grain size.

Credit Author Statement

Filippo Verdolin is the primary contributor. All other authors have provided contributions in terms of writing, editing, discussing, aiding in calculations, and making figures and tables.

Declaration of Competing Interest

We've disclosed the funding sources in the manuscript, and we believe there is no conflict of interest.

Acknowledgements

This work involved a collaboration between the Nuclear Reactors Group of the Department of Energy of Politecnico di Milano and the BISON team of Idaho National Laboratory (INL), in the framework of the I-NERI initiative. It has been funded by the U.S. Department of Energy Nuclear Energy Office (DOE-NE) and by the Advanced Fuel Campaign (AFC) of the Nuclear Technology Research and Development Program. The authors are grateful to Mr R. Genoni for his help in generating the sample images for the study of the bubble equivalent number. This manuscript has been authored by a contractor of the U.S. Government under Contract DE-AC07-05ID14517.

Supplementary material

Supplementary material associated with this article can be found, in the online version, at 10.1016/j.jnucmat.2020.152728

References

[1] A. Waltar, D. Todd, P. Tsvetkov, Fast Spectrum Reactors, Springer, 2012.
[2] B. Merk, A. Stanculescu, P. Chellapandi, R. Hill, Progress in reliability of fast reactor operation and new trends to increased inherent safety, Appl Energy 147 (2015) 104–116.
[3] D.R. Olander, Fundamental aspects of nuclear reactor fuel elements, Technical Information Center, Energy Research and Development Administration, 1976.
[4] S. Fisher, R. White, P. Cook, S. Bremier, R. Corcoran, R. Stratton, C. Walker, P. Ivison, I. Palmer, Microstructure of irradiated SBR MOX fuel and its relationship to fission gas release, J. Nucl. Mater. 306 (2002) 153–172.
[5] K. Maeda, K. Katsuyama, T. Asaga, Fission gas release in FBR MOX fuel irradiated to high burnup, J. Nucl. Mater. 346 (2) (2005) 244–252.
[6] I. Sato, K. Katsuyama, Y. Arai, Fission gases and helium gas behavior in irradiated mixed oxide fuel pin, J. Nucl. Mater. 416 (2011) 151–157.
[7] R. Parrish, A. Aitkaliyeva, A review of microstructural features in fast reactor mixed oxide fuels, J. Nucl. Mater. (2018).
[8] S. Novascone, P. Medvedev, J.W. Peterson, Y. Zhang, J. Hales, Modeling porosity migration in LWR and fast reactor MOX fuel using the finite element method, J. Nucl. Mater. 508 (2018) 226–236.
[9] F. Nichols, Transport phenomena in nuclear fuels under severe temperature gradients, J. Nucl. Mater. 84 (1) (1979) 1–25, doi:10.1016/0022-3115(79)90147-8.
[10] M. Welland, Matter transport in fast reactor fuels, Comprehensive Nuclear Materials 3 (2012) 629–676, doi:10.1016/B978-0-08-056033-5.00073-2.
[11] R.J. Parrish, F. Cappia, A. Aitkaliyeva, Comparison of the radial effects of burnup on fast reactor mox fuel microstructure and solid fission products, J. Nucl. Mater. 531 (2020) 152003, doi:10.1016/j.jnucmat.2020.152003.
[12] Y.-H. Koo, B.-H. Lee, J.-S. Cheon, D.-S. Sohn, Modeling and parametric studies of the effect of inhomogeneity on fission gas release in LWR MOX fuel, Ann Nucl Energy 29 (3) (2002) 271–286.
[13] L. Luzzi, A. Cammi, V.D. Marcello, S. Lorenzi, D. Pizzocri, P.V. Uffelen, Application of the TRANSURANUS code for the fuel pin design process of the ALFRED reactor, Nucl. Eng. Des. 277 (2014) 173–187.
[14] INSPYRE. http://www.eera-jpnm.eu/inspyre/
[15] Generation IV International Forum, https://www.gen-4.org/gif/jcms/c_9261/home
[16] Fuel Cycle Research & Development, https://www.energy.gov/ne/fuel-cycle-technologies/457fuel-cycle-research-development
[17] G. Pastore, L. Luzzi, V.D. Marcello, P.V. Uffelen, Physics-based modelling of fission gas swelling and release in UO_2 applied to integral fuel rod analysis, Nucl. Eng. Des. 256 (2013) 75–86.
[18] G. Pastore, L. Swiler, J. Hales, S. Novascone, D. Perez, B. Spencer, L. Luzzi, P.V. Uffelen, R. Williamson, Uncertainty and sensitivity analysis of fission gas behavior in engineering-scale fuel modeling, J. Nucl. Mater. 456 (2015) 398–408, doi:10.1016/j.jnucmat.2014.09.077.
[19] R.L. Williamson, J.D. Hales, S.R. Novascone, M.R. Tonks, D.R. Gaston, C.J. Permann, D. Andrš, R.C. Martineau, Multidimensional multiphysics simulation of nuclear fuel behavior, J. Nucl. Mater. 423 (1–3) (2012) 149–163.

[20] C. Baker, The migration of intragranular fission gas bubbles in irradiated uranium dioxide, J. Nucl. Mater. 71 (1) (1977) 117–123, doi:10.1016/0022-3115(77)90195-7.
[21] C. Baker, The fission gas bubble distribution in uranium dioxide from high temperature irradiated SGHWR fuel pins, J. Nucl. Mater. 66 (3) (1977) 283–291, doi:10.1016/0022-3115(77)90117-9.
[22] J.A. Turnbull, R.J. White, C. Wise, The diffusion coefficient for fission gas atoms in uranium dioxide, IAEA-TC-699/3.5 (1988).
[23] M.V. Speight, A calculation on the migration of fission gas in material exhibiting precipitation and re-solution of gas atoms under irradiation, Nucl. Sci. Eng. 37 (2) (1969) 180–185, doi:10.13182/NSE69-A20676.
[24] M.V. Speight, W.B. Beeré, Vacancy potential and void growth on grain boundaries, in: Metal Science, 9, 1975, pp. 131—140.
[25] R. White, The development of grain-face porosity in irradiated oxide fuel, J. Nucl. Mater. 325 (1) (2004) 61–77.
[26] R. Williamson, K. Gamble, D. Perez, S. Novascone, G. Pastore, R. Gardner, J. Hales, W. Liu, A. Mai, Validating the bison fuel performance code to integral lwr experiments, Nucl. Eng. Des. 301 (2016) 232–244, doi:10.1016/j.nucengdes.2016.02.020.
[27] T. Barani, E. Bruschi, D. Pizzocri, G. Pastore, P.V. Uffelen, R. Williamson, L. Luzzi, Analysis of transient fission gas behaviour in oxide fuel using BISON and TRANSURANUS, J. Nucl. Mater. 486 (2017) 96–110, doi:10.1016/j.jnucmat.2016.10.051.
[28] J.-Y. Colle, J.-P. Hiernaut, T. Wiss, O. Beneš, H. Thiele, D. Papaioannou, V. Rondinella, A. Sasahara, T. Sonoda, R. Konings, Fission product release and microstructure changes of irradiated MOX fuel at high temperatures, J. Nucl. Mater. 442 (1) (2013) 330–340.
[29] P.C. Millett, M.R. Tonks, S. Biner, L. Zhang, K. Chockalingam, Y. Zhang, Phase-field simulation of intergranular bubble growth and percolation in bicrystals, Journal of Nuclear Materials 425 (1) (2012) 130–135, doi:10.1016/j.jnucmat.2011.07.034. Microstructure Properties of Irradiated Materials
[30] L.K. Aagesen, D. Andersson, B.W. Beeler, M.W. Cooper, K.A. Gamble, Y. Miao, G. Pastore, M.R. Tonks, Phase-field simulations of intergranular fission gas bubble behavior in U3Si2 nuclear fuel, J. Nucl. Mater. 541 (2020) 152415, doi:10.1016/j.jnucmat.2020.152415.
[31] J. Turnbull, C. Friskney, J. Findlay, F. Johnson, A. Walter, The diffusion coefficients of gaseous and volatile species during the irradiation of uranium dioxide, J. Nucl. Mater. 107 (2) (1982) 168–184.
[32] J. Ainscough, B. Oldfield, J. Ware, Isothermal grain growth kinetics in sintered UO_2 pellets, J. Nucl. Mater. 49 (2) (1973) 117–128.
[33] L. Gilpin, R. Baker, S. Chastain, Evaluation of the advanced mixed oxide fuel test FO-2 irradiated in Fast Flux Test Facility, Annual meeting of the American Nuclear Society; Atlanta, GA (USA) 4-8 June 4-8, 1989. Westinghouse Hanford Co., Richland, WA (USA)
[34] M. Teague, M. Tonks, S. Novascone, Microstructural modeling of thermal conductivity of high burn-up mixed oxide fuel, J. Nucl. Mater. 444 (1) (2014) 161–169.
[35] T. Shimada, T. Itaki, Y. Nara, Operational experience of experimental fast reactor JOYO driver fuel, International Conference on Reliable Fuels for Liquid Metal Reactors, 1986.
[36] A. Karahan, Modeling of thermo-mechanical and irradiation behavior of metallic and oxide fuels for sodium fast reactors, Massachusetts Institute of Technology, 2009 Ph.D. thesis. https://tinyurl.com/y72vqvbn
[37] M. Ishida, Y. Korei, Modeling and parametric studies of the effect of pu-mixing heterogeneity on fission gas release from mixed oxide fuels of LWRs and FBRs, J. Nucl. Mater. 210 (1) (1994) 203–215.